Relationship Between Macular Ganglion Cell Thickness and Ocular Elongation as Measured by Axial Length and Retinal Artery Position

Takashi Omoto,[1,2] Hiroshi Murata,[1] Yuri Fujino,[1,9,11] Masato Matsuura,[1] Takashi Fujishiro,[1] Kazunori Hirasawa,[3] Takehiro Yamashita,[4] Takashi Kanamoto,[5] Atsuya Miki,[6] Yoko Ikeda,[7] Kazuhiko Mori,[7,8] Masaki Tanito,[9] Kenji Inoue,[10] Junkichi Yamagami,[2] and Ryo Asaoka[1,11,12]

[1]Department of Ophthalmology, University of Tokyo Graduate School of Medicine, Bunkyo-ku, Tokyo, Japan
[2]Department of Ophthalmology, JR Tokyo General Hospital, Shibuya-ku, Tokyo, Japan
[3]Department of Ophthalmology, School of Medicine, Kitasato University, Minami-ku, Sagamihara-shi Kanagawa, Japan
[4]Department of Ophthalmology, Kagoshima University Graduate School of Medical and Dental Sciences, Sakuragaoka, Kagoshima, Japan
[5]Department of Ophthalmology, Hiroshima Prefectural Hospital, Minami-ku, Hiroshima, Japan
[6]Department of Ophthalmology, Osaka University Graduate School of Medicine, Suita-shi, Osaka, Japan
[7]Department of Ophthalmology, Kyoto Prefectural University of Medicine, Kawaramachi-Hirokoji, Kajii-cho, Kamigyo-ku, Kyoto, Japan
[8]Oike-Ikeda Eye Clinic, Kyoto, Japan
[9]Department of Ophthalmology, Shimane University Faculty of Medicine, Matsue-shi, Shimane, Japan
[10]Inouye Eye Hospital, Chiyoda-ku, Tokyo, Japan
[11]Department of Ophthalmology, Seirei Hamamatsu General Hospital, Shizuoka, Hamamatsu, Japan
[12]Seirei Christopher University, Shizuoka, Hamamatsu, Japan

Correspondence: Ryo Asaoka, Department of Ophthalmology, University of Tokyo Graduate School of Medicine, 7-3-1 Hongo, Bunkyo-ku, Tokyo, 113-8655, Japan; rasaoka-tky@umin.ac.jp.

Received: October 25, 2019
Accepted: August 12, 2020
Published: September 11, 2020

Citation: Omoto T, Murata H, Fujino Y, et al. Relationship between macular ganglion cell thickness and ocular elongation as measured by axial length and retinal artery position. *Invest Ophthalmol Vis Sci.* 2020;61(11):16. https://doi.org/10.1167/iovs.61.11.16

Purpose. We recently reported on the usefulness of retinal artery trajectory in estimating the magnitude of retinal stretch due to myopia. The purpose of the present study was to elucidate the relationship between the peripapillary retinal artery angle (PRAA) and thickness of the macular ganglion cell–inner plexiform layer (GCIPL).

Methods. This r included 138 healthy eyes of 79 subjects older than 20 years of age without any known eye disease. GCIPL thickness was separated into eight sectors according to quadrant and eccentricity from the fovea. The PRAA was calculated as the angle between the superior and inferior retinal arteries. Relationships between whole GCIPL thickness (average and sectorial) and the values of PRAA and axial length (AL) were investigated using a linear mixed model.

Results. Average GCIPL thickness in the whole scanned area decreased significantly with narrowing of the PRAA with and without adjusting for AL. Sectorized macular GCIPL thickness also decreased significantly, with narrowing of the PRAA in seven out of the eight with the adjustment of AL, the exception being the inferior peripheral temporal sector.

Conclusions. Macular GCIPL thickness decreased significantly with narrowing of the PRAA on average and in seven out of eight sectors.

Keywords: glaucoma, myopia, optical coherence tomography, ganglion cell, retinal artery

Optical coherence tomography (OCT) has enabled the in vivo observation of retinal layers, which is useful in assessing various pathological statuses of the eye. The macular ganglion cell–inner plexiform layer (GCIPL), the macular retinal nerve fiber layer (RNFL), and the circumpapillary retinal nerve fiber layer (cpRNFL) are elements that are useful to evaluate when determining the degree of glaucomatous retinal change.[1–6] In particular, the assessment of macular GCIPL thickness is important, as they are the cells primarily damaged by the disease; however, inter-individual variations in the thickness of the GCIPL exist related to various ocular factors, such as myopia,[7–9] which can make diagnosing glaucoma using OCT inaccurate.[10–12] Also, myopia is a known risk factor for the development of glaucoma.[13–15] Therefore, it is important to understand the effects of myopia on structural changes, such as those that occur in GCIPL thickness as measured with OCT.

Previous studies have suggested that macular GCIPL thickness becomes thinner with elongation of the axial length (AL).[16–18] AL is frequently used to estimate the elongation of an eye due to myopia[19,20]; however, we recently reported that the magnitude of associated retinal stretch cannot fully be explained by AL alone, probably due to the large variation of AL inherited at birth across individuals.

Even when two eyes have identical ALs as adults, if their ALs were different at birth then the degree of elongation must have differed between these eyes during the growth period.[21] One of the characteristic findings in such eyes is that supra- and infratemporal thick retinal nerve fiber bundles and retinal vessel trajectory shift toward the fovea in a manner associated with myopic retinal deformation.[22–26] Our earlier research revealed that retinal vessel trajectory was significantly correlated with the RNF bundle trajectory ($R = 0.92$).[22,26] In contrast with AL, the effect of these shifts on the thickness of GCIPL has not yet been investigated; therefore, the aim of the current study was to investigate the relationship between retinal artery angle and macular GCIPL thickness.

Methods

This study was approved by the research ethics committee of the Graduate School of Medicine and Faculty of Medicine at the University of Tokyo. All patients provided written consent for their information to be stored in the hospital database and to be used for research. This study was performed according to the tenets of the Declaration of Helsinki.

Participants

Participants were recruited from medical staffs who were working in any of three hospitals (University of Tokyo Hospital, Hiroshima Prefectural Hospital, and Inouye Eye Hospital; $n = 56$) or subjects who came to each hospital for the purpose of screening for any ocular disease but turned out to be normal based on the results of ophthalmic examinations including slit-lamp biomicroscopy, funduscopy, and intraocular pressure measurements ($n = 23$). The inclusion criteria for the healthy eyes were as follows: (1) no abnormal findings, except for clinically insignificant senile cataract on biomicroscopy, gonioscopy, and fundoscopy; (2) no history of ocular diseases, such as diabetic retinopathy, that could affect the results of OCT examinations; (3) 20 years of age or older; and (4) intraocular pressure of less than 21 mm Hg. Eyes with anomalous discs and diagnosis of glaucoma were cautiously excluded. The signs of glaucomatous changes were judged comprehensively, such as focal rim notching or generalized rim thinning, large cup-to-disc ratio with cup excavation with or without laminar dot sign, and retinal nerve fiber layer defects with edges at the optic nerve head margin and disc edge hemorrhages, according to the recommendations of the Japan Glaucoma Society Guidelines for Glaucoma.[27] Eyes with past ophthalmic surgeries except for uncomplicated cataract surgery were also excluded.

OCT Measurement

GCIPL thicknesses were obtained using an OCT device (RS 3000; Nidek Co., Ltd., Aichi, Japan). OCT imaging was performed after pupil dilation with combined eye drops of 0.5% tropicamide and 0.5% phenylephrine hydrochloride (Midrin-P; Santen Pharmaceutical Co., Ltd., Osaka, Japan). The raster scan protocol for 30 degrees of visual angle (128 × 512 pixels) was used for all scans, and the data in the central 8.1-mm square were used in the analysis. The magnification effect was corrected according to the manufacturer-provided formula based on Littman's equation,[28,29] using the measured AL value. Data with a signal strength index of greater than 7 were included in the current analysis. Images that were unclear due to eye movements or involuntary blinking were acquired again or carefully excluded. In addition, all of the boundaries were checked, and eyes with segmentation errors were carefully excluded from the study. All 65,536 (128 × 512) A-scan pixels of GCIPL thickness were exported for each eye, and those in the analysis area were divided into 10 × 10 grids, then stratified into eight sectors according to the quadrant and the eccentricity from the fovea (Fig. 1). The data obtained in the left eye were mirror-imaged to those obtained in the right eye for statistical analysis.

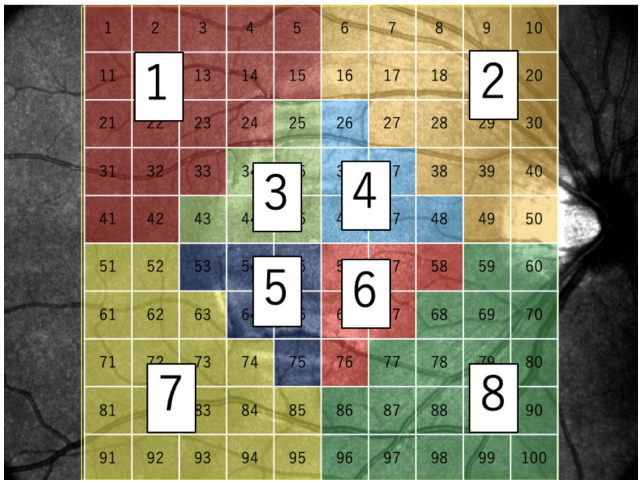

Figure 1. Macular grids and sectors. Macular (8.1-mm square) 10 × 10 grids were stratified into eight sectors according to the quadrant and the eccentricity from the fovea. The left eye was mirror imaged.

The positions of major retinal arteries in the superotemporal and inferotemporal areas were determined by identifying the points where the retinal artery and the 3.4-mm-diameter cpRNFL scan circle overlapped using ImageJ 1.48 (National Institutes of Health, Bethesda, MD, USA). The peripapillary retinal arteries angle (PRAA) was the angle between the superior and inferior retinal arteries (Fig. 2).

Statistical Analysis

First, the relationship between AL and PRAA was investigated using a linear mixed model approach in which the random effect was the subject, with and without adjusting for age. Then, the relationship between average GCIPL thickness in the whole scanned area and the values of AL and PRAA were investigated using a multivariate linear mixed model in which the random effect was the subject, with and without adjusting for age. Similarly, at each sector, the relationships between GCIPL thickness (derived from 10 × 10 grids) and the values of AL and PRAA were investigated using a multivariate linear mixed model in which the random effect was the subjects, with and without adjusting for age. The linear mixed model is equivalent to ordinary linear regression in that the model describes the relationship between the predictor variables and a single outcome variable; however, standard linear regression analysis makes the assumption that all observations are independent of each other. In the current study, measurements were

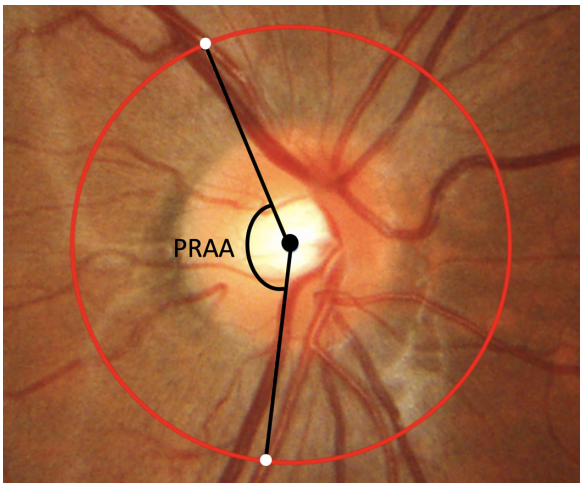

Figure 2. Measurement of the right-eye PRAA. The PRAA was calculated by identifying the angle between the intersecting positions (*white dots*) of a 3.4-mm-diameter peripapillary scan circle (*red*) and the supratemporal/infratemporal major retinal arteries.

Table 1. Study Subject Demographics

Demographic	Value
Eyes (right, left), *n*	70, 68
Subjects (female, male), *n*	56, 23
Age (y), mean ± SD	42.3 ± 18.4
AL (mm), mean ± SD	24.6 ± 1.3
PRAA (°), mean ± SD	135.9 ± 20.7
GCIPL (μm), mean ± SD	
Average	54.3 ± 5.2
Sector 1	42.3 ± 6.4
Sector 2	51.9 ± 5.8
Sector 3	77.7 ± 7.0
Sector 4	80.7 ± 7.0
Sector 5	78.1 ± 6.7
Sector 6	78.7 ± 6.4
Sector 7	43.0 ± 6.0
Sector 8	49.1 ± 5.3

nested within subjects and, thus, dependent on each other. Ignoring this grouping of the measurements would result in an underestimation of standard errors of the regression coefficients. The linear mixed model adjusts for the hierarchical structure of the data, modeling in a way in which measurements are grouped within subjects to reduce the possible bias of including both eyes of one patient.[30,31] Benjamini and Hochberg's method was used to adjust for multiple comparisons.[32] Statistical significance was set at 0.05. All analyses were performed using R 3.5.2 (R Foundation for Statistical Computing, Vienna, Austria).

Results

Table 1 presents the demographic details for the subjects. Of the 138 healthy eyes studied, 70 eyes were right eyes and 68 eyes were left eyes. Twenty-three subjects were male, and 56 subjects were female. The mean ± SD age was 42.3 ± 18.4 years. The mean AL was 24.6 ± 1.3 mm, and the mean PRAA was 135.9 ± 20.7°.

Figure 3 shows the relationship between AL and PRAA. Of note, there was a significant relationship between the two

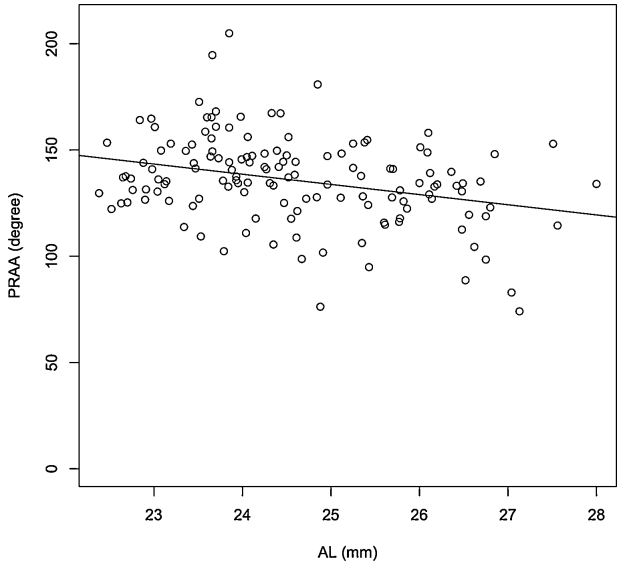

Figure 3. Scatterplot of AL and PRAA. There was a significant relationship between AL and PRAA.

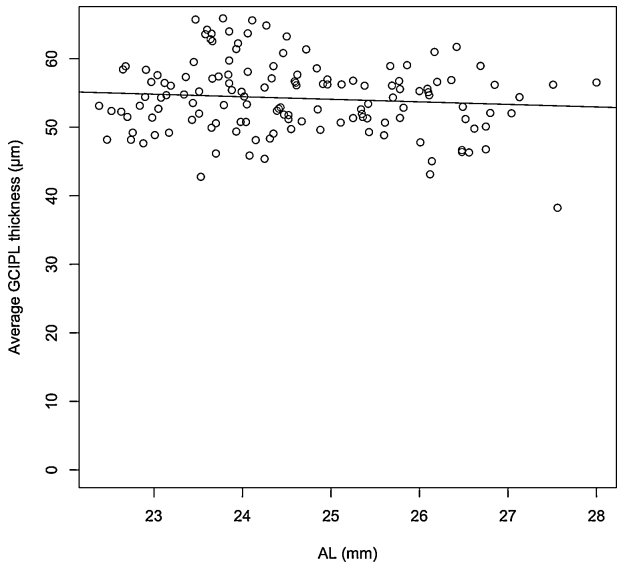

Figure 4. Scatterplots of AL and average GCIPL thickness in the whole scanned area. There was not a significant relationship between AL and average GCIPL thickness.

values (coefficient = –4.8; $P = 0.0021$, linear mixed model). This was not largely changed with the adjustment for age (coefficient = –4.7; $P = 0.0040$).

The average GCIPL thickness in the whole scanned area was not significantly related with AL (coefficient = –0.37; $P = 0.34$, linear mixed model) (Fig. 4). This did not change when adjusted for age (coefficient = –0.53; $P = 0.19$); however, the average GCIPL thickness in the whole scanned area decreased significantly with narrowing of the PRAA (coefficient = 0.050; $P < 0.001$, linear mixed model) (Fig. 5). A very similar relationship was observed with the adjustment for age (coefficient = 0.052; $P < 0.001$). Multivariate linear mixed model analysis also revealed that PRAA was significantly related to average GCIPL thickness

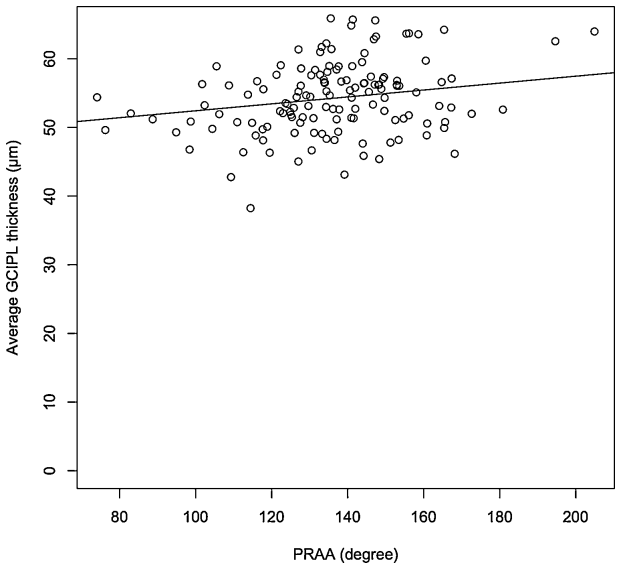

Figure 5. Scatterplots of PRAA and average GCIPL thickness in the whole scanned area. There was a significant relationship between PRAA and average GCIPL thickness (linear mixed model).

Table 2. Relationship Between Sectorial GCIPL Thickness and AL and PRAA Values, Not Adjusted for Age

	AL		PRAA	
Sector	Coefficient (μm/mm)	*P*	Coefficient (μm/degree)	*P*
1	0.54	0.69	0.069	0.0087*
2	−0.37	0.69	0.043	0.027*
3	−0.22	0.69	0.072	0.0087*
4	−0.31	0.69	0.069	0.0046*
5	−0.47	0.69	0.078	0.0046*
6	−0.26	0.69	0.062	0.0046*
7	−0.21	0.69	0.034	0.067
8	−0.83	0.34	0.042	0.023*

* $P < 0.05$.

Table 3. Relationship Between Sectorial GCIPL Thickness and AL and PRAA Values, Adjusted for Age

	AL		PRAA	
Sector	Coefficient (μm/mm)	*P*	Coefficient (μm/degree)	*P*
1	0.38	0.50	0.069	0.0067*
2	−0.59	0.39	0.044	0.024*
3	−0.57	0.40	0.074	0.0067*
4	−0.66	0.39	0.071	0.0032*
5	−0.72	0.39	0.078	0.0032*
6	−0.56	0.39	0.064	0.0032*
7	−0.32	0.50	0.034	0.063
8	−0.93	0.23	0.043	0.021*

*$P < 0.05$.

(coefficient = 0.050; $P < 0.001$, adjusted for age), but AL was not (coefficient = –0.36; $P = 0.35$, adjusted for age).

Tables 2 and 3 show the relationship between GCIPL thickness and the values of AL and PRAA for each sector, using the multivariate linear mixed model, without (Table 2) or with (Table 3) adjustment for age. GCIPL thickness was not significantly related to AL at all sectors ($P > 0.05$, multivariate linear mixed model with adjustment for multiple comparisons), with and without the adjustment for age. In contrast, GCIPL thickness decreased significantly with the decrease in the PRAA in all sectors, except for sector 7 ($P < 0.05$, multivariate linear mixed model with adjustment for multiple comparisons), with and without the adjustment for age.

Discussion

In the current study, the relationships between macular GCIPL thickness and the values of AL and PRAA were investigated in 138 eyes of 79 participants without ocular pathology. The results indicate that macular GCIPL thickness decreased significantly with narrowing of the PRAA in seven out of eight sectors. This finding was not observed for GCIPL thickness and AL. Interestingly, AL was not significantly related to macular GCIPL thickness, either in total area or in each sector, in the study. This finding contrasts with many other previous reports suggesting that GCIPL thickness decreases with elongation of AL.[7,8,16–18,33] This may be because most of the previous studies did not account for the magnification effect,[7,8,16–18] and more peripheral retina was analyzed in eyes with long AL. Of note, Mwanza et al.[7] estimated the influence of the magnification effect on the thickness of GCIPL in detail and suggested that this influence was large enough to even reverse the effect of AL on GCIPL thickness from negative to positive. In contrast, a previous study has suggested a significant effect of AL on GCIPL thickness, even after correcting for the magnification effect. Araie et al.[33] investigated this association in a circular retinal area with a diameter of 0.6 mm (corresponding to approximately 2 degrees of visual angle) with correction for the magnification effect and observed that the GCIPL thickness decreased with a decrease in spherical equivalent refractive error. This contradictory result compared with the current study may be attributed to differences in the study settings. For example, the area of analysis was much wider in the current study (8.1-mm square), because the purpose of the study was to investigate the association between PRAA and GCIPL thickness. By comparison, in the study by Araie et al.,[33] the purpose was to evaluate the correlation between retinal sensitivities of the innermost four test points with the Humphrey Field Analyzer (HFA) 24–2 test and corresponding GCIPL thickness in normal eyes. In addition, spherical equivalent refractive error was used in the previous study, whereas the AL value itself was used in the current study.

In contrast to AL, the current study suggested that there was a significant negative relationship between PRAA and macular GCIPL thickness, agreeing with our previous reports.[22,26,34] In our previous work,[22] the distribution of cpRNFL fibers through the thickest peaks of cpRNFL coincided well with that of the retinal artery trajectory ($R = 0.92$). A clinical merit of utilizing PRAA or retinal artery trajectory versus the cpRNFL peak angle is that, in glaucoma patients, the cpRNFL thickness profile changes during the disease process, whereas the PRAA does not. Indeed, we have previously reported that adjusting the cpRNFL profile using the retinal artery angle significantly improved the structure–function relationship,[35] suggesting that it is useful to consider the retinal artery trajectory when assessing the cpRNFL profile in eyes with glaucoma. However, the current study found that macular GCIPL thickness was also significantly decreased with narrowing of the PRAA. This suggests that careful consideration of the PRAA is also key when

Investigative Ophthalmology & Visual Science

assessing GCIPL thickness in eyes with glaucoma. In a future study, the effects of PRAA on the structure–function relationship and diagnosis should be investigated in patients with glaucoma. Furthermore, we previously reported the usefulness of applying a random forests machine learning method to macular-grid GCIPL thicknesses when diagnosing early-onset glaucoma.[36] It would be of interest, as well, to investigate whether adding PRAA information to this further improves the diagnostic accuracy.

GCIPL thickness decreased with narrowing of the PRAA in seven sectors but not in one sector in the inferior temporal area (sector 2) (Tables 2 and 3). The reason for this result is not clear, but it does suggest that a different tendency occurs in terms of macular retinal deformation associated with elongation of the eye in the superior and inferior hemiretinae, particularly near the optic disc. In the paper by Hood et al.,[37] the RNFL stream was traced and the corresponding angle on the optic disc was identified. The authors suggested that the RNFL from the inferior temporal optic disc angle runs closer to the macula as compared to that from the superior temporal optic disc angle because of the position of the optic disc superior to the macula. We also validated this result with regard to the structure–function relationship,[38] as the PRAA superior to the papillomacular bundle (70.6°) was larger than the PRAA inferior to the papillomacular bundle (64.6°) in the current study (data not shown in the Results section). This difference may be related to the various relationships between the PRAA and GCIPL thickness between the superior and inferior hemiretinae. Indeed, peripapillary atrophy and choroidal thinning are other findings that develop in association with the elongation of an eyeball,[39–41] and they are usually predominantly observed in the inferior hemiretina near the optic disc.[42–44] This also suggests that different macular retinal deformation profiles are associated with the elongation of an eye between the superior and inferior hemiretinae. These differing macular retinal deformation profiles between the superior and inferior hemiretinae are important to consider not only when investigating the mechanisms of retinal deformation due to myopia but also when elucidating the pathological mechanisms of glaucoma in myopic eyes, because a visual field defect is usually predominant in the inferior hemifield in myopic glaucomatous eyes.[45–47] It should be noted, however, that the association between GCIPL thickness and PRAA was significant, but not very strong, as suggested by the relatively large *P* value (from 0.0032 to 0.027). Thus, PRAA has an effect on the GCLIPL thickness, but it does not explain all of the variation of GCIPL thickness in healthy subjects.

Araie et al.[33] reported a correlation between visual field sensitivity and macular GCIPL thickness in normal eyes. In addition, previous studies have suggested that cpRNFL thickness tended to increase as standard automated perimetric sensitivity increased in normal eyes, although the slope did not reach a level of significance.[3,48] On the other hand, there are conflicting reports suggesting that spatial[49–51] and temporal[50,52] contrast sensitivity is normal or reduced in myopic eyes.[53] It would be of interest to investigate the effects on visual function of GCIPL thinning associated with narrowing retinal arteries.

We previously reported that a narrow PRAA is related to poor damping capacity of an eye as measured with the Ocular Response Analyzer (Reichert Technologies, Depew, NY, USA) or OCULUS Corvis STL (Oculus, Inc., Menlo Park, CA, USA).[54,55] Such damping capacity of an eye has been reported to be associated with the development and progression of glaucoma and other retinal diseases such as angioid streaks.[56–58] We have speculated that eyes are deformed even in daily life activities, such as postural changes, eyelid blinking, ocular pulsatility due to ocular hemodynamics, performing the Valsalva maneuver, and regular eye movement.[59–61] Eyes with poor damping capacity (poor hysteresis) are not able to absorb these external strains, which could contribute to the development of ocular diseases. Such poor damping capacity and thin GCIPLs in eyes with narrow angles could raise the likelihood of developing glaucoma, which may, at least in part, explain why myopia is a risk factor for the development of glaucoma.[62]

Recently, another independent determinant of macular layer thickness was reported: disk fovea distance. [63,64] We investigated the effect of this variable on GCIPL thickness, but we did not find a significant association utilizing whole field and sector-wise analyses (data not shown in Results). This may be due to differences in the populations analyzed; the previous studies either analyzed total retinal thickness (GCIPL in this study)[64] or excluded myopic eyes with spherical equivalent less than –6.0 diopters.[63]

One of the limitations of the current study was the small number of highly myopic eyes. A more evident tendency than shown in this study could perhaps be observed in a larger population. On the other hand, the current results suggest that thinning of the GCIPL thickness associated with narrowing of the artery angle is significant even in a non-highly myopic cohort.

In conclusion, macular GCIPL thickness decreased significantly with narrowing of the PRAA in addition to elongation of the AL on average and in seven out of eight sectors.

Acknowledgments

The authors thank Enago (www.enago.jp) for the English language review.

Supported in part by grants from the Ministry of Education, Culture, Sports, Science and Technology of Japan (25861618 to HM; 19H01114, 18KK0253, 26462679 to RA; 20768254 to YF; 00768351 to MM) and by the Suzuken Memorial Foundation and Mitsui Life Social Welfare Foundation.

Disclosure: **T. Omoto**, None; **H. Murata**, None; **Y. Fujino**, None; **M. Matsuura**, None; **T. Fujishiro**, None; **K. Hirasawa**, None; **T. Yamashita**, None; **T. Kanamoto**, None; **A. Miki**, None; **Y. Ikeda**, None; **K. Mori**, None; **M. Tanito**, None; **K. Inoue**, None; **J. Yamagami**, None; **R. Asaoka**, None

References

1. Tan O, Chopra V, Lu AT, et al. Detection of macular ganglion cell loss in glaucoma by Fourier-domain optical coherence tomography. *Ophthalmology*. 2009;116:2305–2314.e2.
2. Kim NR, Lee ES, Seong GJ, Kim JH, An HG, Kim CY. Structure-function relationship and diagnostic value of macular ganglion cell complex measurement using Fourier-domain OCT in glaucoma. *Invest Ophthalmol Vis Sci*. 2010;51:4646–4651.
3. Cho JW, Sung KR, Lee S, et al. Relationship between visual field sensitivity and macular ganglion cell complex thickness as measured by spectral-domain optical coherence tomography. *Invest Ophthalmol Vis Sci*. 2010;51:6401–6407.
4. Li S, Wang X, Li S, Wu G, Wang N. Evaluation of optic nerve head and retinal nerve fiber layer in early and advance glaucoma using frequency-domain optical coherence tomography. *Graefes Arch Clin Exp Ophthalmol*. 2010;248:429–434.

5. Schulze A, Lamparter J, Pfeiffer N, Berisha F, Schmidtmann I, Hoffmann EM. Diagnostic ability of retinal ganglion cell complex, retinal nerve fiber layer, and optic nerve head measurements by Fourier-domain optical coherence tomography. *Graefes Arch Clin Exp Ophthalmol*. 2011;249:1039–1045.
6. Hood DC. Improving our understanding, and detection, of glaucomatous damage: an approach based upon optical coherence tomography (OCT). *Prog Retin Eye Res*. 2017;57:46–75.
7. Mwanza JC, Durbin MK, Budenz DL, et al. Profile and predictors of normal ganglion cell-inner plexiform layer thickness measured with frequency-domain optical coherence tomography. *Invest Ophthalmol Vis Sci*. 2011;52:7872–7879.
8. Seo S, Lee CE, Jeong JH, Park KH, Kim DM, Jeoung JW. Ganglion cell-inner plexiform layer and retinal nerve fiber layer thickness according to myopia and optic disc area: a quantitative and three-dimensional analysis. *BMC Ophthalmol*. 2017;17:22.
9. Sezgin Akcay BI, Gunay BO, Kardes E, Unlu C, Ergin A. Evaluation of the ganglion cell complex and retinal nerve fiber layer in low, moderate, and high myopia: a study by RTVue spectral domain optical coherence tomography. *Semin Ophthalmol*. 2017;32:682–688.
10. Shoji T, Nagaoka Y, Sato H, Chihara E. Impact of high myopia on the performance of SD-OCT parameters to detect glaucoma. *Graefes Arch Clin Exp Ophthalmol*. 2012;250:1843–1849.
11. Choi YJ, Jeoung JW, Park KH, Kim DM. Glaucoma detection ability of ganglion cell-inner plexiform layer thickness by spectral-domain optical coherence tomography in high myopia. *Invest Ophthalmol Vis Sci*. 2013;54:2296–2304.
12. Akashi A, Kanamori A, Ueda K, Inoue Y, Yamada Y, Nakamura M. The ability of SD-OCT to differentiate early glaucoma with high myopia from highly myopic controls and nonhighly myopic controls. *Invest Ophthalmol Vis Sci*. 2015;56:6573–6580.
13. Xu L, Wang Y, Wang S, Wang Y, Jonas JB. High myopia and glaucoma susceptibility the Beijing Eye Study. *Ophthalmology*. 2007;114:216–220.
14. Qiu M, Wang SY, Singh K, Lin SC. Association between myopia and glaucoma in the United States population. *Invest Ophthalmol Vis Sci*. 2013;54:830–835.
15. Jonas JB, Aung T, Bourne RR, Bron AM, Ritch R, Panda-Jonas S. Glaucoma. *Lancet*. 2017;390:2183–2193.
16. Koh VT, Tham YC, Cheung CY, et al. Determinants of ganglion cell-inner plexiform layer thickness measured by high-definition optical coherence tomography. *Invest Ophthalmol Vis Sci*. 2012;53:5853–5859.
17. Nouri-Mahdavi K, Nowroozizadeh S, Nassiri N, et al. Macular ganglion cell/inner plexiform layer measurements by spectral domain optical coherence tomography for detection of early glaucoma and comparison to retinal nerve fiber layer measurements. *Am J Ophthalmol*. 2013;156:1297–307.e2.
18. Totan Y, Guragac FB, Guler E. Evaluation of the retinal ganglion cell layer thickness in healthy Turkish children. *J Glaucoma*. 2015;24:e103–e108.
19. Morgan IG, Ohno-Matsui K, Saw S-M. Myopia. *Lancet*. 2012;379:1739–1748.
20. Benjamin B, Davey J, Sheridan M, Sorsby A, Tanner J. Emmetropia and its aberrations; a study in the correlation of the optical components of the eye. *Spec Rep Ser Med Res Counc (G B)*. 1957;11:1–69.
21. Axer-Siegel R, Herscovici Z, Davidson S, Linder N, Sherf I, Snir M. Early structural status of the eyes of healthy term neonates conceived by in vitro fertilization or conceived naturally. *Invest Ophthalmol Vis Sci*. 2007;48:5454–5458.
22. Yamashita T, Asaoka R, Tanaka M, et al. Relationship between position of peak retinal nerve fiber layer thickness and retinal arteries on sectoral retinal nerve fiber layer thickness. *Invest Ophthalmol Vis Sci*. 2013;54:5481–5488.
23. Yoo YC, Lee CM, Park JH. Changes in peripapillary retinal nerve fiber layer distribution by axial length. *Optom Vis Sci*. 2012;89:4–11.
24. Hong SW, Ahn MD, Kang SH, Im SK. Analysis of peripapillary retinal nerve fiber distribution in normal young adults. *Invest Ophthalmol Vis Sci*. 2010;51:3515–3523.
25. Kim JM, Park KH, Kim SJ, et al. Comparison of localized retinal nerve fiber layer defects in highly myopic, myopic, and non-myopic patients with normal-tension glaucoma: a retrospective cross-sectional study. *BMC Ophthalmol*. 2013;13:67.
26. Yamashita T, Sakamoto T, Terasaki H, Tanaka M, Kii Y, Nakao K. Quantification of retinal nerve fiber and retinal artery trajectories using second-order polynomial equation and its association with axial length. *Invest Ophthalmol Vis Sci*. 2014;55:5176–5182.
27. Japan Glaucoma Society. [The Japan Glaucoma Society Guidelines for Glaucoma (4th Edition)]. *Nippon Ganka Gakkai Zasshi*. 2018;122:3–53.
28. Littman H. Zur Bestimmung der wahren Größe eines Objektes auf dem Hintergrund des lebenden Auges. *Klin Monatsbl Augenheilkd*. 1982;180:286–289.
29. Littman H. Zur Bestimmung der wahren Größe eines Objektes auf dem Hintergrund eines lebenden Auges. *Klin Monatsbl Augenheilkd*. 1988;192:66–67.
30. Baayen RH, Davidson DJ, Bates DM. Mixed-effects modeling with crossed random effects for subjects and items. *J Mem Lang*. 2008;59:390–412.
31. Bates D, Mächler M, Bolker B, Walker S. Fitting linear mixed-effects models using lme4. *J Stat Soft*. 2015;67:1–48.
32. Benjamini Y, Hochberg Y. Controlling the false discovery rate: a practical and powerful approach to multiple testing. *J R Stat Soc Ser B Methodol*. 1995;57:289–300.
33. Araie M, Saito H, Tomidokoro A, Murata H, Iwase A. Relationship between macular inner retinal layer thickness and corresponding retinal sensitivity in normal eyes. *Invest Ophthalmol Vis Sci*. 2014;55:7199–7205.
34. Yamashita T, Terasaki H, Yoshihara N, Kii Y, Uchino E, Sakamoto T. Relationship between retinal artery trajectory and axial length in Japanese school students. *Jpn J Ophthalmol*. 2018;62:315–320.
35. Fujino Y, Yamashita T, Murata H, Asaoka R. Adjusting circumpapillary retinal nerve fiber layer profile using retinal artery position improves the structure-function relationship in glaucoma. *Invest Ophthalmol Vis Sci*. 2016;57:3152–3158.
36. Asaoka R, Hirasawa K, Iwase A, et al. Validating the usefulness of the "random forests" classifier to diagnose early glaucoma with optical coherence tomography. *Am J Ophthalmol*. 2017;174:95–103.
37. Hood DC, Raza AS, de Moraes CG, Liebmann JM, Ritch R. Glaucomatous damage of the macula. *Prog Retin Eye Res*. 2013;32C:1–21.
38. Fujino Y, Murata H, Matsuura M, et al. Mapping the central 10 degrees visual field to the optic nerve head using the structure-function relationship. *Invest Ophthalmol Vis Sci*. 2018;59:2801–2807.
39. Jonas JB, Gusek GC, Naumann GO. Optic disk morphometry in high myopia. *Graefes Arch Clin Exp Ophthalmol*. 1988;226:587–590.
40. Akagi T, Hangai M, Kimura Y, et al. Peripapillary scleral deformation and retinal nerve fiber damage in high myopia assessed with swept-source optical coherence tomography. *Am J Ophthalmol*. 2013;155:927–936.
41. Ramrattan RS, Wolfs RC, Jonas JB, Hofman A, de Jong PT. Determinants of optic disc characteristics in a general population: the Rotterdam Study. *Ophthalmology*. 1999;106:1588–1596.

Investigative Ophthalmology & Visual Science

42. Ho J, Branchini L, Regatieri C, Krishnan C, Fujimoto JG, Duker JS. Analysis of normal peripapillary choroidal thickness via spectral domain optical coherence tomography. *Ophthalmology*. 2011;118:2001–2007.
43. Tanabe H, Ito Y, Terasaki H. Choroid is thinner in inferior region of optic disks of normal eyes. *Retina*. 2012;32:134–139.
44. Gupta P, Cheung CY, Saw SM, et al. Peripapillary choroidal thickness in young Asians with high myopia. *Invest Ophthalmol Vis Sci*. 2015;56:1475–1481.
45. Araie M, Arai M, Koseki N, Suzuki Y. Influence of myopic refraction on visual field defects in normal tension and primary open angle glaucoma. *Jpn J Ophthalmol*. 1995;39:60–64.
46. Mayama C, Suzuki Y, Araie M, et al. Myopia and advanced-stage open-angle glaucoma. *Ophthalmology*. 2002;109:2072–2077.
47. Kimura Y, Hangai M, Morooka S, et al. Retinal nerve fiber layer defects in highly myopic eyes with early glaucoma. *Invest Ophthalmol Vis Sci*. 2012;53:6472–6478.
48. Alasil T, Wang K, Yu F, et al. Correlation of retinal nerve fiber layer thickness and visual fields in glaucoma: a broken stick model. *Am J Ophthalmol*. 2014;157:953–959.
49. Fiorentini A, Maffei L. Spatial contrast sensitivity of myopic subjects. *Vision Res*. 1976;16:437–438.
50. Thorn F, Corwin TR, Comerford JP. High myopia does not affect contrast sensitivity. *Curr Eye Res*. 1986;5:635–639.
51. Collins JW, Carney LG. Visual performance in high myopia. *Curr Eye Res*. 1990;9:217–223.
52. Chen PC, Woung LC, Yang CF. Modulation transfer function and critical flicker frequency in high-myopia patients. *J Formos Med Assoc*. 2000;99:45–48.
53. Jaworski A, Gentle A, Zele AJ, Vingrys AJ, McBrien NA. Altered visual sensitivity in axial high myopia: a local postreceptoral phenomenon? *Invest Ophthalmol Vis Sci*. 2006;47:3695–3702.
54. Asano S, Asaoka R, Yamashita T, et al. Relationship between the shift of the retinal artery associated with myopia and ocular response analyzer waveform parameters. *Transl Vis Sci Technol*. 2019;8:15.
55. Asano S, Asaoka R, Yamashita T, et al. Correlation between the myopic retinal deformation and corneal biomechanical characteristics measured with the Corvis ST tonometry. *Transl Vis Sci Technol*. 2019;8:26.
56. Matsuura M, Hirasawa K, Murata H, Nakakura S, Kiuchi Y, Asaoka R. The usefulness of CorvisST tonometry and the Ocular Response Analyzer to assess the progression of glaucoma. *Sci Rep*. 2017;7:40798.
57. Hirasawa K, Matsuura M, Murata H, et al. Association between corneal biomechanical properties with ocular response analyzer and also CorvisST tonometry, and glaucomatous visual field severity. *Transl Vis Sci Technol*. 2017;6:18.
58. Asano S, Nakajima K, Kure K, et al. Corneal biomechanical properties are associated with the activity and prognosis of angioid streaks. *Sci Rep*. 2018;8:8130.
59. Singh K, Dion C, Wajszilber M, Ozaki T, Lesk MR, Costantino S. Measurement of ocular fundus pulsation in healthy subjects using a novel Fourier-domain optical coherence tomography. *Invest Ophthalmol Vis Sci*. 2011;52:8927–8932.
60. Kim YW, Girard MJ, Mari JM, Jeoung JW. Anterior displacement of lamina cribrosa during valsalva maneuver in young healthy eyes. *PLoS One*. 2016;11:e0159663.
61. Wang X, Rumpel H, Lim WE, et al. Finite element analysis predicts large optic nerve head strains during horizontal eye movements. *Invest Ophthalmol Vis Sci*. 2016;57:2452–2462.
62. Mitchell P, Hourihan F, Sandbach J, Wang JJ. The relationship between glaucoma and myopia: the Blue Mountains Eye Study. *Ophthalmology*. 1999;106:2010–2015.
63. Qiu K, Chen B, Yang J, et al. Effect of optic disc-fovea distance on the normative classifications of macular inner retinal layers as assessed with OCT in healthy subjects. *Br J Ophthalmol*. 2019;103:821–825.
64. Qiu K, Wang G, Zhang R, Lu X, Zhang M, Jansonius NM. Influence of optic disc-fovea distance on macular thickness measurements with OCT in healthy myopic eyes. *Sci Rep*. 2018;8:5233.

Investigative Ophthalmology & Visual Science